Vaccinia virus-mediated melanin production allows MR and optoacoustic deep tissue imaging and laser-induced thermotherapy of cancer

Jochen Stritzker[a,b,1], Lorenz Kirscher[b], Miriam Scadeng[c], Nikolaos C. Deliolanis[d,e], Stefan Morscher[d,f], Panagiotis Symvoulidis[d], Karin Schaefer[d], Qian Zhang[a], Lisa Buckel[b], Michael Hess[b], Ulrike Donat[b], William G. Bradley[g], Vasilis Ntziachristos[d], and Aladar A. Szalay[a,b,h,1]

[a]Genelux, San Diego, CA 92109; [b]Department of Biochemistry, Biocenter, University of Würzburg, 97074 Würzburg, Germany; [c]Center for Functional MRI, University of California at San Diego, La Jolla, CA 92093; [d]Institute for Biological and Medical Imaging, Helmholtz Zentrum München and Technische Universität München, 85764 Neuherberg, Germany; [e]Fraunhofer Project Group for Automation in Medicine and Biotechnology, 68167 Mannheim, Germany; [f]iThera Medical, 85764 Neuherberg, Germany; [g]Department of Radiology, University of California at San Diego Medical Center, San Diego, CA 92103; and [h]Department of Radiation Oncology, Moores Cancer Center, University of California at San Diego, La Jolla, CA 92093

Edited* by Roger Y. Tsien, University of California at San Diego, La Jolla, CA, and approved January 14, 2013 (received for review October 1, 2012)

We reported earlier the delivery of antiangiogenic single chain antibodies by using oncolytic vaccinia virus strains to enhance their therapeutic efficacy. Here, we provide evidence that gene-evoked production of melanin can be used as a therapeutic and diagnostic mediator, as exemplified by insertion of only one or two genes into the genome of an oncolytic vaccinia virus strain. We found that produced melanin is an excellent reporter for optical imaging without addition of substrate. Melanin production also facilitated deep tissue optoacoustic imaging as well as MRI. In addition, melanin was shown to be a suitable target for laser-induced thermotherapy and enhanced oncolytic viral therapy. In conclusion, melanin as a mediator for thermotherapy and reporter for different imaging modalities may soon become a versatile alternative to replace fluorescent proteins also in other biological systems. After ongoing extensive preclinical studies, melanin overproducing oncolytic virus strains might be used in clinical trials in patients with cancer.

translational medicine | personalized medicine | diagnosis | photoacoustic | whole-body imaging

Theranostics are considered a key to personalized medicine combining therapy and diagnosis in a single agent. However, "stand-alone" theranostics resulting from engineered gene expression have not been developed yet. Theranostic agents are generally comprised of dual/multifunctional nanoparticles that can be visualized noninvasively in real time by an imaging modality and at the same time are loaded with (chemo-)therapeutic agents. Some of these particles have also been equipped with molecules that enable their targeting of specific receptors (e.g., arthritis and cancer). However, most of them still need to be improved in terms of specificity as well as increased concentrations at the target site.

Insertion of reporter genes to oncolytic viruses resulted in another class of theranostic agents. Oncolytic viruses are characterized by their largely tumor cell-specific replication, resulting in tumor cell lysis and efficient tumor regression. Tumor selectivity is an inherent property of a number of viruses such as Newcastle disease virus, parvovirus, and vaccinia virus. These could be enhanced, for example, by deletion of viral genes, which are dispensable in malignant cells, or by production of surface receptors that bind ligands that are highly expressed on tumor cells (1).

The vaccinia virus strain GLV-1h68 was effective in treating more than 40 tumor xenograft models in mice, shown to be safe in a recently completed phase I trial upon systemic injection to human cancer patients (2), and is currently undergoing several additional phase I/II trials (www.clinicaltrials.gov). This strain also carries genes that allow optical detection via GFP and *Renilla* luciferase expression (3) and further encodes enzymes (β-gal and glucuronidase) that can be monitored in the serum of tumor-bearing mice (4) as well as in the blood of humans with cancer. In addition, it was shown to enhance the therapeutic effect of this oncolytic vaccinia virus strain when an antiangiogenic single-chain antibody was encoded by the virus (5). Here, the oncolytic vaccinia virus strain GLV-1h68 served as backbone for the insertion of key genes in melanogenesis. We speculated that introduction of melanogenesis into tumor cells might render them visible as a result of melanin overproduction by optical as well as optoacoustic imaging (6) and might facilitate therapy. Furthermore, it is well known that melanotic melanomas generate high signal on T1-weighted magnetic resonance images (7, 8), probably as a result of trapping of paramagnetic transition metal ions (9). Previously published cell culture data also encouraged us to use the production of melanin as a reporter for MRI (9–11). Targeted melanin overproduction as a reporter for optoacoustic imaging or MRI in live animals or humans has not yet been established. The goal therefore was to use the vaccinia virus strain GLV-1h68 as an example for a vehicle equipped with genes for melanin overproduction and use the produced melanin as an (additional) theranostic mediator.

Results

Gene-Evoked Melanin Production. In a pilot study, cDNAs of the key enzymes in melanogenesis, namely tyrosinase (*Tyr*), tyrosinase-related protein 1 (*Tyrp1*), and dopachrome tautomerase (*DCT*; also known as *Tyrp2*) were inserted into a mammalian expression vector. Production of melanin in HeLa cells was observed only when the tyrosinase encoding plasmid DNA was introduced (Fig. S1). Cotransformation of the *Tyrp1* plasmid resulted in production of a darker (eu-)melanin (12), whereas DCT expression did not seem to have any influence on the produced melanin. Therefore, tyrosinase alone, or in combination with *Tyrp1*, was inserted into the vaccinia virus genome under control of a synthetic early (SE) or the much stronger synthetic early/late (SEL) promoter. Upon infection with the newly generated recombinant vaccinia virus (rVACV) strains, cells produced significant amounts of melanin (Fig. 1*A*). Optical density measurements of

Author contributions: J.S., M.S., N.C.D., and V.N. designed research; J.S., L.K., M.S., N.C.D., S.M., P.S., K.S., M.H., and U.D. performed research; J.S., L.K., M.S., N.C.D., S.M., P.S., Q.Z., L.B., U.D., and V.N. contributed new reagents/analytic tools; J.S., L.K., M.S., N.C.D., S.M., P.S., K.S., and A.A.S. analyzed data; and J.S., M.S., N.C.D., S.M., Q.Z., W.G.B., and A.A.S. wrote the paper.

Conflict of interest statement: J.S., Q.Z. and A.A.S. are employees and shareholders of Genelux. S.M. is an employee of iThera Medical.

*This Direct Submission article had a prearranged editor.

Freely available online through the PNAS open access option.

[1]To whom correspondence may be addressed. E-mail: js@genelux.com or aaszalay@genelux.com.

This article contains supporting information online at www.pnas.org/lookup/suppl/doi:10.1073/pnas.1216916110/-/DCSupplemental.

infected cell suspensions (Fig. 1*B*) confirmed what was already visible in the cell pellets: Low amounts of tyrosinase (under control of the SE-promoter) resulted in a light brown coloration of the cells whereas high amounts of tyrosinase (SEL–promoter constructs) led to much darker infected cells.

The darkest (i.e., coal black) cells were consistently observed upon GLV-1h324 infection. Obviously, the additional coexpression of Tyrp1 in low amounts could increase the biosynthesis of the black eumelanin. So far, 16 of 16 tested tumor cell lines (including cells from different cancers and different species) produced melanin when infected with the melanin-rVACV strains. Interestingly, melanin in infected red-fluorescent protein expressing PC-3 (PC-3-RFP) cells almost completely suppressed the RFP fluorescence signal (Fig. S2), probably by absorption of excitation and emission light.

The influence of melanin production on viral replication and virus-mediated cell lysis was determined by measuring the activity of the virus-encoded glucuronidase in cell lysates and in the cell culture supernatant, respectively (4). It was shown that higher amounts of melanin seemed to inhibit viral replication at later time points during infection (Fig. S3*A*). However, melanin did not significantly influence viral cell lysis, which also was confirmed by a cell viability assay (Fig. S3 *B* and *C*). More importantly, the melanin-rVACV strains retained their oncolytic activity, although A549 tumor regression was decelerated compared with the control-rVACV strain GLV-1h68 (Fig. S3*D*). Of note, the net body weight (tumor weight subtracted from whole body weight) as a marker for "well-being" was somewhat higher in the melanin-rVACV groups, even though this was not statistically significant (Fig. S3*D*, *Inset*). Analyses of isolated tumor tissues from perfused mice at the end of the experiments clearly demonstrated that melanin-rVACV colonized tumors, in contrast to controls, produced so much melanin that they appeared coal-black (Fig. S3*E*).

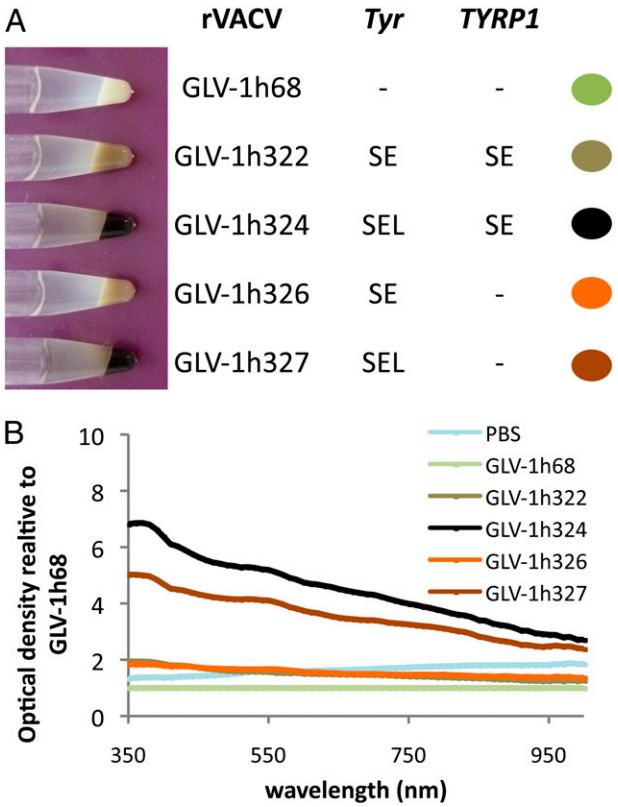

Fig. 1. Production of melanin upon key enzyme expression. (*A*) Pellets of infected CV-1 cells and overview of the infecting rVACV strains encoding Tyr and/or Tyrp1 under control of a weaker SE or strong SEL promoter. The colored dots indicate the color used for each strain in all following figures. (*B*) Optical density measurements over the spectrum from 350 nm to 1,000 nm (in 5-nm increments) were conducted, and the relative optical density compared with the results obtained with GLV-1h68 infected A549 cells was plotted for each data point.

Near-IR Laser-Induced Thermotherapy of Melanin Producing Tumors. As the produced melanin also significantly enhances the absorption of light in the so-called near-IR optical window, which is characterized by low absorption and maximum light penetration in tissues (13), we tested whether we could use a near-IR laser to specifically transfer energy to melanin. The transferred energy would then be converted to thermal energy, eventually heating the melanin-producing cells (and cells in their vicinity) to temperatures causing protein denaturation and cell death, and therefore enabling thermotherapy. Fig. 2 shows that we achieved this by using an 808-nm laser: Whereas mock-infected or control-rVACV–infected tumor cell suspensions warmed up by only approximately 3 °C during 2 min of exposure to the laser light, the melanin-rVACV cell suspension temperature increased by 25 °C for GLV-1h327– and by 41 °C for GLV-1h324–infected cells, respectively, resulting in a temperature higher than 65 °C (Fig. 2*A*, *Upper*). Accordingly, the 120-s laser treatment killed almost all cells in the GLV-1h324–infected aliquot (Fig. 2*A*, *Lower*). When using a single 2-min laser treatment on A549 tumor-bearing mice, the skin on top of the laser-exposed tumor section changed its color (most likely because of the heat inside the tumor underneath) when melanin was expressed in the tumor beneath (Fig. 2*B*), but not in the control-rVACV–injected mice. Tumor size measurements 1 and 5 d after laser therapy revealed the success of this thermotherapy: Whereas the GLV-1h68 control groups did not show significant differences in terms of tumor volume changes, the laser treatment did reduce the tumor volume significantly in GLV-1h324–treated mice compared with tumors that were not exposed to the laser light (Fig. 2*C*). The virus-mediated melanin production in infected tumor cells therefore facilitates near-IR–assisted thermotherapy in addition to the oncolytic virotherapy. Similar results were also achieved by using the B16F10 melanoma cell line (Fig. S4), which naturally produces melanin.

Optoacoustic Imaging of Melanin-Producing Tumors and Metastases. Optoacoustic imaging is an emerging in vivo imaging technology (14, 15), whereby short light energy pulses are absorbed by tissue and converted to thermal energy and subsequently to ultrasound signals that allow high-resolution whole-body imaging. The oncolytic virus mediated production of melanin and its optical absorption in the near-IR enables the imaging of tumors and metastases with this modality. Pellets of cells infected with various melanin-rVACV strains (Fig. 3*A*), for different time points post infection (Fig. 3*B*) and at different dilutions (Fig. 3*C*) showed optoacoustic signals in the near-IR range that were equivalent to optical absorption up to 2 cm^{-1}. These values are one order of magnitude above the 0.3- to 0.5-cm^{-1} tissue optical absorption in near-IR and are comparable with the 2-cm^{-1} absorption of whole blood, thus ensuring sufficient signal to background ratio. In combination with multispectral optoacoustic tomographic (MSOT) imaging of melanin-containing tumors, we were able to generate an image processing algorithm that allowed us to specifically visualize the presence and distribution of melanin not only on the surface but also deep within the mouse body (Fig. S5). With this technique, surface near A549 and PC-3 tumors as well as PC-3-RFP lymph node metastases (Figs. 3 *D* and *E* and S6), which, in a recent study, were shown to be preferentially colonized vs. the primary tumor (16), could be detected in live mice injected with melanin-rVACV.

MR Imaging of Tumors and Metastases upon Melanin Production. Knowing we can produce high amounts of melanin specifically in colonized tumors, we analyzed whether the virus-mediated melanin production would also lead to signal intensity changes in

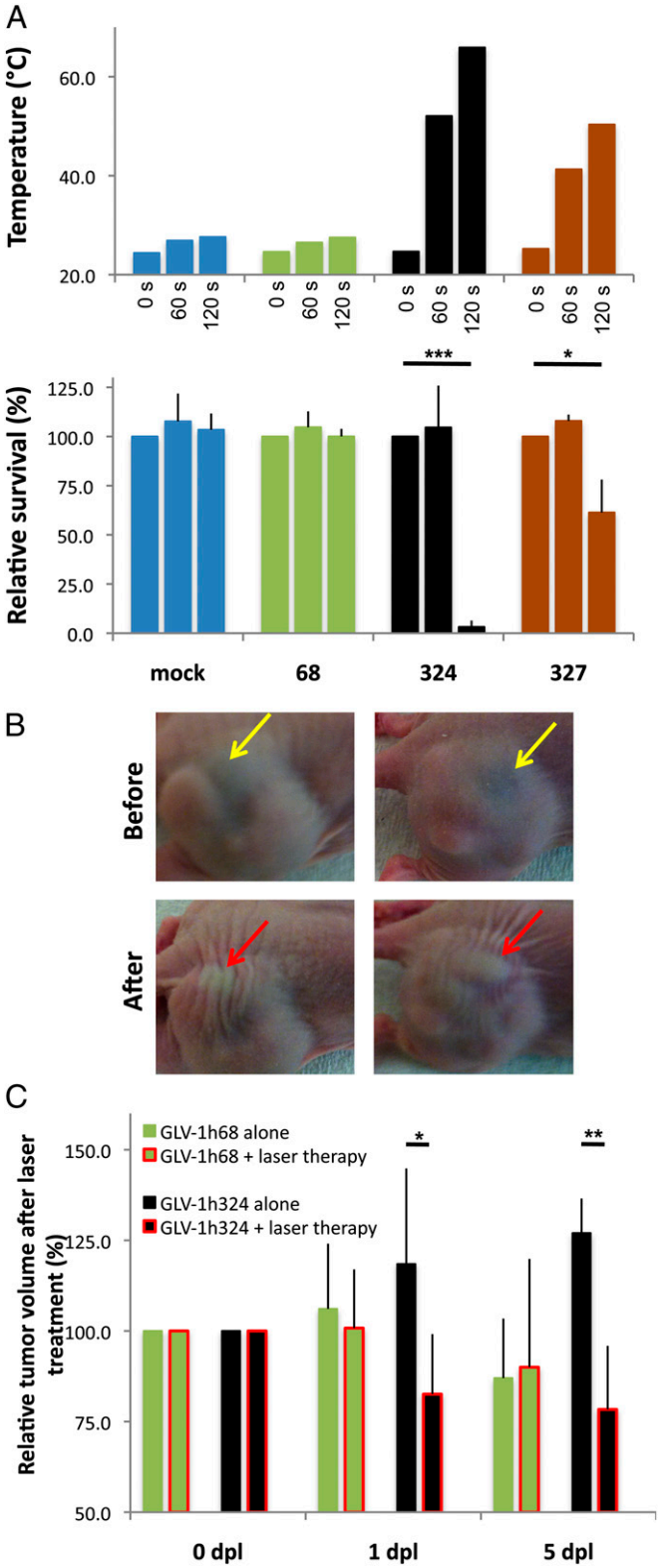

Fig. 2. Melanin biosynthesis facilitates near-IR laser-induced thermotherapy. (*A*) A549 cell suspensions were exposed to 808 nm laser light for 0, 60, and 120 s, respectively. (*Upper*) Measured temperature (in °C) immediately after laser treatment. (*Lower*) Relative survival compared with each non–laser-light–exposed sample (*$P < 0.05$, ***$P < 0.0001$). (*B*) Photographs of laser-treated, melanin-rVACV–injected mice before (*Upper*) and immediately after treatment (*Lower*). The area that was exposed to laser light is indicated by a yellow arrow. The red arrows indicate the same area where tissue damage was observed after treatment. (*C*) Tumor size measurements revealed significant differences in tumor size between the laser-treated and untreated GLV-1h324 subgroups at 1 and 5 d post laser treatment (dpl). No significant differences were observed in the GLV-1h68 subgroups (*$P < 0.05$, **$P < 0.005$).

MR imaging, which, unlike optical imaging, is not alleviated in deep tissues. Indeed, we found a markedly shortened T1 relaxation time when PC-3-RFP or A549 cells were infected with the melanin-rVAVC, but not with GLV-1h68 (Fig. 4 *A* and *C*). Similar to the data already found in optical and optoacoustic analysis, the greatest T1 shortening was also observed by using the GLV-1h324 strain. To determine the lower detection limit, we analyzed twofold serial dilutions of GLV-1h324–infected cells in noninfected A549 cells (Fig. 4*B*). Although no changes were observed when one in 128 cells produced melanin (T1, 1,954 ± 15 ms vs. 1,940 ± 11 ms for noninfected cells), the 1:64-fold dilution significantly reduced the T1 relaxation time (1,860 ± 16 ms). Higher concentration of GLV-1h324–infected cells further decreased T1 relaxation times. When looking at how early T1 relaxation changes occurred after infection, we already found significant reductions after only 24 h post infection, which were even more pronounced after 48 h (Fig. 4*C*). More detailed analysis of GLV-1h324–infected cells revealed a significant T1 shortening after 18 h, but not 12 h, post infection, correlating to what was already observed for the optoacoustic signal (Fig. 3*D*).

Most importantly, the melanin-dependent T1-relaxation changes could be used to generate increased signal in MRI of melanin-rVACV–colonized tumors in live mice (Fig. 4*D*). Although tumors of the control-rVACV–injected mice appeared evenly gray, the melanin-rVACV–colonized A549 tumors were characterized by regions of very high signal (almost white when using the same contrast settings as for the control mice). Moreover, these regions of high signal intensity correlated very well with the melanin distribution in the tumor that could be visualized on the cryosections of the same mice. Tumor regions that (at this time) did not produce melanin because the oncolytic rVACV did not (yet) infect this part of the tumor showed a similar gray level as the tumors of the control mice. Quantitative analysis of T1 maps (Fig. S7) confirmed T1 relaxation time reduction in the melanin-rVACV– compared with control-rVACV–injected mice tumor tissue, but not muscle (Fig. 4*E*).

Consequently, we wanted to know whether we would be able to detect not only relatively large tumors (as shown by the A549 model), but also the smaller PC-3-RFP lymph node metastases. In this study, metastases colonized with melanin-rVACV were shown to exhibit increased intensity in MRI of live mice (Fig. S8) whereas lymph node metastases of PBS solution- or control-rVACV–injected mice had similar gray levels as the primary tumor. The colocalization of increased intensity in MRI and presence of melanin was demonstrated after perfusion and dissection of the mice. Furthermore, immunohistochemistry was used to confirm the presence of rVACV in the lymph node metastases (Fig. S8), demonstrating that melanin was actually produced intracellularly in the metastasized lymph nodes and not transported as free melanin into these structures from the primary tumor.

In addition to the in vivo MR imaging experiments described earlier, we performed MRI analysis of isolated A549 tumors in a clinical 3-T MR instrument to demonstrate that use of melanin production as a reporter could be translated to clinical settings (Fig. S9).

Discussion

Here, we have shown that simple gene-evoked melanin production has the potential to become widely used in several diagnostic (e.g., marker during surgery, for endoscopy, in optoacoustic and MR imaging) as well as in therapeutic (e.g., near-IR light-induced thermotherapy) procedures in the clinic. Whether Tyrp1 should be

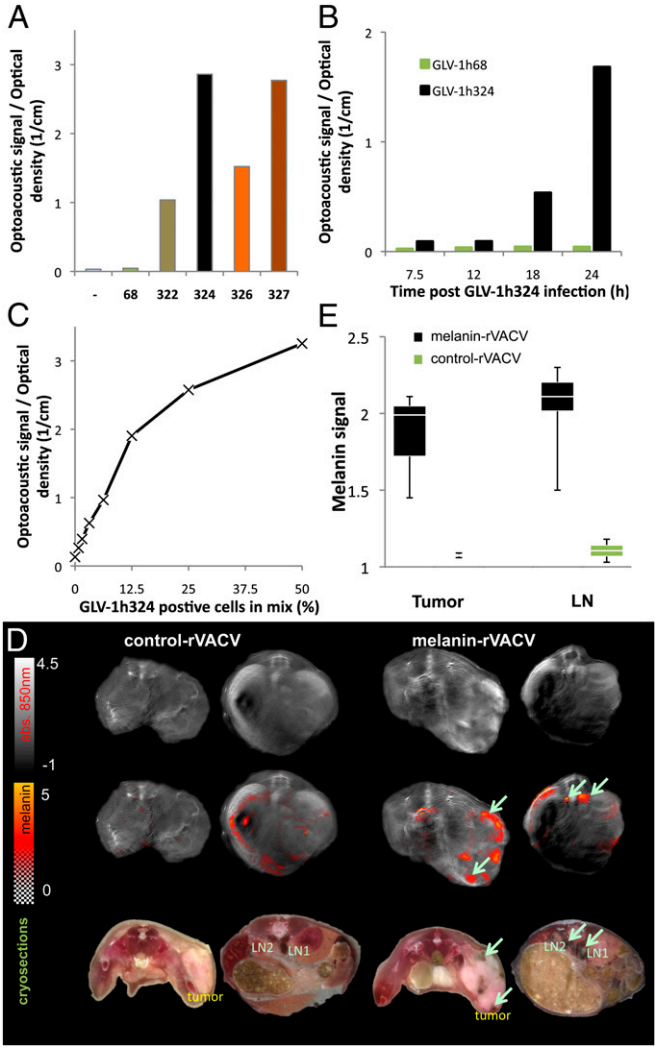

Fig. 3. Optoacoustic imaging of melanin-rVACV in cell cultures and in live mice. (*A*) Three days after infection, PC-3-RFP cell suspensions were analyzed for their optoacoustic signals, which were strongest in GLV-1h324 and GLV-1h327–infected cells. (*B*) Infected A549 cells were analyzed at different times post infection. For GLV-1h324–infected A549 cells, a significant optoacoustic signal increase was observed at 18 h post infection. (*C*) GLV-1h324 infected A549 cells were diluted in uninfected cells and the optoacoustic signal determined. Even at the lowest concentration (one in 128 cells), an optoacoustic signal was detected that was significantly higher than that of control cells. (*D*) MSOT of PC-3-RFP tumor and lymph node metastasis (LN1 and LN2) bearing live mice 14 d after rVACV injection. (*Top*) Background optoacoustic images taken at 850 nm excitation wavelength. (*Middle*) Melanin spatial distribution (pseudocolor) is overlaid on the background images (*Top*) using a variable transparency function as shown in the color bar. The melanin signature was picked up in the melanin-rVACV–injected mice which correlated with the distribution of melanin in the corresponding cryosections (*Bottom*) as indicated by the arrows. (*E*) Quantitative optoacoustic signal intensities for melanin in tumors and lymph nodes as box and whisker plots for three melanin- and two control-VACV–injected mice.

coexpressed in addition to tyrosinase for enhanced eumelanin production in vivo will probably be dependent on the model. Although we detected significant differences in (eu-)melanin production in cell culture, Tyrp1 did not have obvious advantages in virus-colonized tumor models in terms of melanin production. The darker color of eumelanin results in better MSOT contrast, and therefore Tyrp1 coexpression should help when Tyr expression results in pheomelanin biosynthesis. Eumelanin is known to have more efficient binding capacity for certain drugs and metal ions (17), and might also have more potential in storing iron compared with pheomelanin (18). Therefore, eumelanin might give a better MR signal, and, consequently, Tyrp1 expression could be

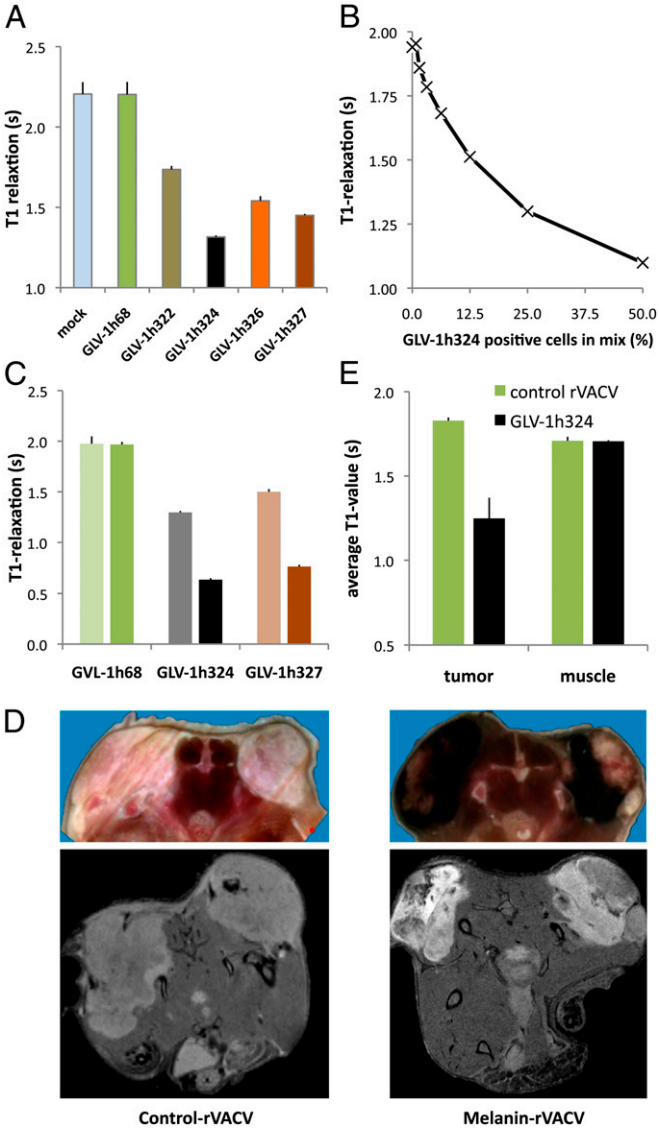

Fig. 4. The production of melanin resulted in bright signal on a T1-weighted MR image by causing T1 shortening. (*A*) T1-relaxation times of harvested PC-3-RFP cell suspensions 3 d after infection. (*B*) Mixtures of GLV-1h324 infected with noninfected A549 cells showed significant T1-relaxation time shortening in the 1:64 dilution (1.56% of infected A549 cells) compared with noninfected A549. (*C*) At 24 h (light colored bars) and 48 h post infection, the T1-relaxtion time was significantly shortened in the melanin-rVACV infected cells, with more decrease at the later time point. (*D*) The grayscale pictures illustrate representative T1-weighted images of live A549 tumor-bearing mice that were injected with GLV-1h68 and GLV-1h324 strains, respectively. The two tumors in each mouse are clearly visible but much brighter in the melanin-rVACV colonized tumors as a result of T1 shortening. (*Upper*) Images obtained after cryoslicing of the same mice show approximately the same section that can be seen on the MR images (*Lower*). The bright regions in the MR images correspond very well with the black melanin areas that were observed in the cryosections of the GLV-1h324–injected mouse, whereas no melanin containing regions in the same tumors appeared as dark as the tumor in MR images of the control mouse. (*E*) The average T1-relaxtion time plus SD of tumors and muscle (control) from two mice in each group was obtained from T1 maps of individual slices.

advantageous in models that do not allow the production of tyrosinase and/or melanin in high concentrations. Compared with fluorescent proteins, melanin can certainly not be used for subcellular protein distribution and interaction analysis, but it has the advantage of being visible by noninvasive deep tissue imaging with MSOT and MRI. In addition, the detection of fluorescent proteins is probably more sensitive than melanin in terms of generated signal per molecule, but melanin is produced enzymatically by the expressed enzyme(s), which allows relatively fast detection by MRI (in our case within 18 h post viral cell infection) with increasing intensity over time. Other advantages vs. fluorescent proteins are the extreme stability of melanin (19), the lack of tissue autofluorescence (in fact, autofluorescence is reduced by melanin, which is another way of detecting the melanin), as well as the fact that no special equipment is needed to visualize the dark pigments. Finally, the ubiquitous presence of melanin in all kingdoms of life suggests that introduction of melanin synthesis as diagnostic/theragnostic marker will be possible in most species, e.g., including plants (20), and should also find translation into clinical settings.

Materials and Methods

Tyrosinase and Tyrp1 expressing melanin-rVACV were constructed using guanine phosphoribosyltransferase selection (21). Optical absorption of cell suspensions was determined in 10-nm increments from 350 nm to 1,000 nm. For MSOT experiments, image acquisition at 11 wavelengths in 15-nm intervals starting from 700 nm and up to 850 nm enabled separation of absorbers with distinct spectral absorption profiles. Melanin distribution could be determined by separating out the background signal of deoxygenated and oxygenated hemoglobin that dominate the contrast in tissue. T1-weighted MRI (multislice–multiecho sequence; repetition time, 927 ms; echo time, 10.6 ms; four excitations; matrix, 256 × 256; field of view, 2.8 cm; slice thickness, 0.5mm; 35 slices) of live mice was performed on a 7-T small animal imaging system. T1 relaxation time maps were acquired on a single slice through the center of the tumors. Thermotherapy of melanin containing material was initiated by a 2-min exposure to 808 nm near-IR laser beam (beam diameter, 5 × 8 mm; laser power, 2.00 W). Detailed experimental procedures are provided in *SI Materials and Methods*.

All animal experiments were carried out in accordance with protocols approved by the Regierung von Unterfranken (Würzburg, Germany; Protocol AZ 55.2–2531.01–17/08) and/or the Institutional Animal Care and Use Committee of Explora BioLabs (located in the San Diego Science Center, San Diego, CA; Protocol EB11-025) and/or the Institutional Animal Care and Use Committee of the University of California at San Diego (Protocol R08335).

ACKNOWLEDGMENTS. The authors thank Jason Aguilar, Sarah Glasl, Uwe Klemm, Johanna Langbein-Laugwitz, and Terry Trevino for their technical assistance and Stanislav Emelianov for helpful discussion. This work was supported by Genelux, iThera Medical, a Service Grant awarded to the University of Würzburg, a Bundesministeriums für Bildung und Forschung Go-Bio award (to V.N.), graduate stipends from the University of Würzburg (to L.K., L.B., and M.H.), a postdoctoral fellowship (to U.D.) from a Research Service Grant awarded by Genelux Corporation to the University of Würzburg, and a European Research Council Senior Investigator Award (to V.N.).

1. Bourke MG, et al. (2011) The emerging role of viruses in the treatment of solid tumours. *Cancer Treat Rev* 37(8):618–632.
2. Pedersen JV, et al. (2011) A phase I clinical trial of a genetically modified and imageable oncolytic vaccinia virus GL-ONC1 with clinical green fluorescent protein (GFP) imaging. *J Clin Oncol* 29(suppl):abstr. 2577.
3. Zhang Q, et al. (2007) Eradication of solid human breast tumors in nude mice with an intravenously injected light-emitting oncolytic vaccinia virus. *Cancer Res* 67(20): 10038–10046.
4. Hess M, et al. (2011) Bacterial glucuronidase as general marker for oncolytic virotherapy or other biological therapies. *J Transl Med* 9:172.
5. Frentzen A, et al. (2009) Anti-VEGF single-chain antibody GLAF-1 encoded by oncolytic vaccinia virus significantly enhances antitumor therapy. *Proc Natl Acad Sci USA* 106(31):12915–12920.
6. Krumholz A, et al. (2011) Photoacoustic microscopy of tyrosinase reporter gene in vivo. *J Biomed Opt* 16(8):080503.
7. Premkumar A, et al. (1996) Metastatic melanoma: Correlation of MRI characteristics and histopathology. *J Magn Reson Imaging* 6(1):190–194.
8. DeJordy JO, Bendel P, Horowitz A, Salomon Y, Degani H (1992) Correlation of MR imaging and histologic findings in mouse melanoma. *J Magn Reson Imaging* 2(6):695–700.
9. Enochs WS, Petherick P, Bogdanova A, Mohr U, Weissleder R (1997) Paramagnetic metal scavenging by melanin: MR imaging. *Radiology* 204(2):417–423.
10. Paproski RJ, Forbrich AE, Wachowicz K, Hitt MM, Zemp RJ (2011) Tyrosinase as a dual reporter gene for both photoacoustic and magnetic resonance imaging. *Biomed Opt Express* 2(4):771–780.
11. Weissleder R, et al. (1997) MR imaging and scintigraphy of gene expression through melanin induction. *Radiology* 204(2):425–429.
12. Slominski A, Tobin DJ, Shibahara S, Wortsman J (2004) Melanin pigmentation in mammalian skin and its hormonal regulation. *Physiol Rev* 84(4):1155–1228.
13. Jöbsis FF (1977) Noninvasive, infrared monitoring of cerebral and myocardial oxygen sufficiency and circulatory parameters. *Science* 198(4323):1264–1267.
14. Ntziachristos V (2010) Going deeper than microscopy: The optical imaging frontier in biology. *Nat Methods* 7(8):603–614.
15. Wang LV, Hu S (2012) Photoacoustic tomography: In vivo imaging from organelles to organs. *Science* 335(6075):1458–1462.
16. Donat U, et al. (2012) Preferential colonization of metastases by oncolytic vaccinia virus strain GLV-1h68 in a human PC-3 prostate cancer model in nude mice. *PLoS ONE* 7(9):e45942.
17. Mårs U, Larsson BS (1999) Pheomelanin as a binding site for drugs and chemicals. *Pigment Cell Res* 12(4):266–274.
18. Ito S (2006) Encapsulation of a reactive core in neuromelanin. *Proc Natl Acad Sci USA* 103(40):14647–14648.
19. Glass K, et al. (2012) Direct chemical evidence for eumelanin pigment from the Jurassic period. *Proc Natl Acad Sci USA* 109(26):10218–10223.
20. Borisjuk L, Rolletschek H, Neuberger T (2012) Surveying the plant's world by magnetic resonance imaging. *Plant J* 70(1):129–146.
21. Falkner FG, Moss B (1988) Escherichia coli gpt gene provides dominant selection for vaccinia virus open reading frame expression vectors. *J Virol* 62(6):1849–1854.